J. Micromech. Microeng. **17** (2007) 2528–2537 doi:10.1088/0960-1317/17/12/020

A MEMS viscometric sensor for continuous glucose monitoring

Yongjun Zhao[1], Siqi Li[2], Arthur Davidson[3], Bozhi Yang[1], Qian Wang[2] and Qiao Lin[4]

[1] Department of Mechanical Engineering, Carnegie Mellon University, Pittsburgh, PA, USA
[2] Department of Chemistry and Biochemistry and Nanocenter, University of South Carolina, Columbia, SC, USA
[3] Department of Electrical and Computer Engineering, Carnegie Mellon University, Pittsburgh, PA, USA
[4] Department of Mechanical Engineering, Columbia University, New York, NY, USA

E-mail: qlin@columbia.edu

Received 17 July 2007, in final form 23 October 2007
Published 14 November 2007
Online at stacks.iop.org/JMM/17/2528

Abstract
We present a MEMS sensor aiming to enable continuous monitoring of glucose levels in diabetes patients. The device features a magnetically-driven vibrating microcantilever, which is situated in a microchamber and separated from the environment by a semi-permeable membrane. Glucose sensing is based on affinity binding principles using a solution of dextran concanavalin-A (Con A) as the sensing fluid. The glucose concentration is determined by detecting viscosity changes induced by the binding of glucose to Con A through the measurement of the cantilever's vibration parameters. The device is capable of measuring physiologically relevant glucose concentrations from 0 to 25 mM with a resolution better than 0.025 mM and a phase sensitivity better than 0.4° mM^{-1}. The response of the sensor to glucose concentration changes has a time constant down to 4.27 min, and can be further improved with optimized device designs.

(Some figures in this article are in colour only in the electronic version)

1. Introduction

Diabetes mellitus is a metabolic disease characterized by persistent hyperglycemia (high blood sugar levels). Close monitoring of diabetes treatment with repetitive daily blood glucose measurements allows timely identification and correction of problematic blood sugar patterns. This has been demonstrated to reduce the risk of diabetes-related complications.

Continuous glucose monitoring (CGM) allows the most timely detection of abnormal glucose levels, and can be accomplished by either non-invasive or minimally invasive approaches [1]. Non-invasive devices rely on transdermal sampling and detection of glucose in interstitial fluid (ISF) [2, 3], and in general have limited accuracy and reliability. Minimally invasive, subcutaneously implanted devices allow direct and accurate extraction of ISF glucose levels [1–3]. Existing minimally invasive systems are mostly based on electrochemical detection of enzyme-catalyzed reactions [4–9]. While electrochemical methods allow sensitive glucose detection, they have some significant drawbacks. First, glucose is irreversibly consumed during detection. This might change the equilibrium concentration of glucose in tissue, and thus, the actual measured glucose level. Furthermore, the rate of glucose consumption is diffusion limited. Any changes in diffusion layers (e.g. by cell deposition, capsule formation) on the sensor surface affect the diffusion rate, and, thus, the device sensitivity. In addition, drift hydrogen peroxide production and interference from electrode-active chemicals often cause inaccuracies. As a result, electrochemical CGM sensors often exhibit large drifts and require frequent calibration (typically at least once every 12 h [6, 8]). This lack of reliability has been severely hindering CGM applications to practical diabetes treatment.

To overcome these limitations, alternative glucose sensing techniques have been under active investigation. In particular,

methods that use non-consumptive, competitive affinity binding of glucose have shown great promise [10–15]. Such methods are typically based on the solution of a polysaccharide (e.g., dextran) crosslinked by a glucose-binding protein (e.g., concanavalin A or Con A) [10]. When glucose is added to the solution, it binds competitively to Con A and causes reversible de-crosslinking of dextran–Con A complex, which can be detected via the resulting changes in solution properties, such as fluorescence [16, 17] or viscosity [10, 12, 13, 18, 19]. As it is based on equilibrium binding in which glucose is not consumed, affinity sensing is not susceptible to electroactive interferents. More importantly, affinity sensing is considerably more tolerant to biofouling. That is, the deposition of biological material (e.g., cells and proteins) on the implanted affinity sensor surface results only in an increased equilibration time *without* any changes in measurement accuracy. Consequently, affinity glucose sensors can be highly stable and low drift. For example, GlucOnline^{TM}, a device under commercial development and based on viscometry of the Con A/dextran system [20, 21], has demonstrated excellent stability, requiring calibration only once over a 3 day period and allowing sensor readings to be displayed in real time. However, requirements of microdialysis and conventional viscometric instruments make this device rather bulky, cumbersome and expensive.

MEMS technology promises to allow batch fabrication of low-cost implantable sensors that integrate multiple functional components for metabolic monitoring. Such devices are miniaturized, leading to improved measurement time response and minimized invasiveness. MEMS or related technologies have previously been applied for glucose sensors that are based on electrochemical [22–25], eletrophoretic [26], thermal [27–29], optical [30] and colorimetric [31] detection methods. MEMS-based devices have also exploited microdialysis [32, 33] and glucose-induced hydrogel swelling [34]. Here, we present a MEMS-based viscometric sensor that aims to use affinity binding principles to enable continuous glucose monitoring. The sensor utilizes the Con A/dextran system; changes in the solution viscosity caused by glucose/Con A binding are detected using a MEMS vibrational cantilever. We envision that when subcutaneously implanted, the sensor will allow the detection of glucose in interstitial fluid (ISF). There are several distinct advantages to MEMS-based affinity glucose sensing. Compared with electrochemical glucose sensors, it offers the benefits of other affinity sensing techniques, such as tolerance to biofouling and electroactive interferents. Compared to existing affinity-based glucose sensors, the advantages include (1) it is miniaturized with minimal invasiveness and minimized use of sensing solution; (2) it allows integration of functional components for reliable glucose sensing; (3) it can potentially be batch fabricated in an array to empower simultaneous monitoring of multiple metabolites; (4) it eliminates the use of microdialysis, simplifying operation and potentially allowing complete implantation in tissue; and (5) it potentially enables vibration-based active mixing of glucose in the sensing fluid, leading to a rapid response to glucose concentration changes.

The paper is organized as follows. The basic principle and conceptual design are first introduced. A device model and the microfabrication process are then presented. The experimental method and setup are described next, followed by the presentation and discussion of the experimental results. The paper concludes with a summary and a brief discussion of future work.

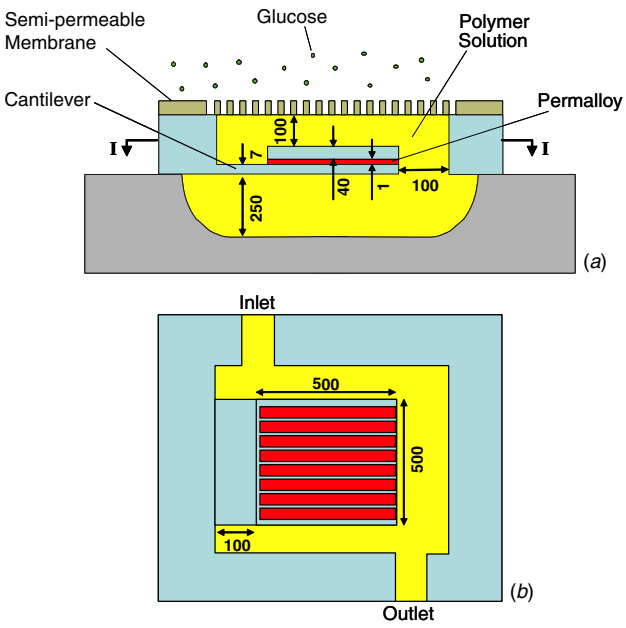

Figure 1. Schematic of the MEMS viscometric glucose sensor: (*a*) cross-sectional view and (*b*) top view of the microchamber looking down from cross-section I–I shown in (*a*). Dimensions shown (in micrometers) are those of the microfabricated prototype devices (section 4).

2. Principle and design

As shown in figure 1, the MEMS viscometric glucose sensor is based on a cantilever situated inside a microchamber. The cantilever is a polymer thin film anchored on the substrate at one end, and suspended over a cavity. Permalloy thin film strips are deposited on the cantilever at its free end, and are covered with a thick reinforcement polymer layer to prevent the curling of the cantilever because of the intrinsic stress mismatch between the polymer and metal thin films. The microchamber is formed between the substrate and a polymer membrane and is filled with a solution of Con A and dextran. The membrane is semi-permeable in that glucose outside the chamber can permeate through the membrane, while neither Con A nor dextran can escape. During operation, the cantilever is set in vibration by a remotely applied magnetic field, which acts on the permalloy strips. The viscosity change, caused by the interaction of glucose that permeates into and out of the chamber with the solution, alters the characteristics of the cantilever vibration, which can be measured to obtain the glucose concentration.

The affinity glucose sensing principle is illustrated in figure 2. The sensing solution consists of dextran, a branched polysaccharide made of glucose units and Con A, a protein that can specifically bind to up to four glucose units reversibly. The dextran molecules can be crosslinked by binding to Con A, forming a highly viscous, gel-like solution. When

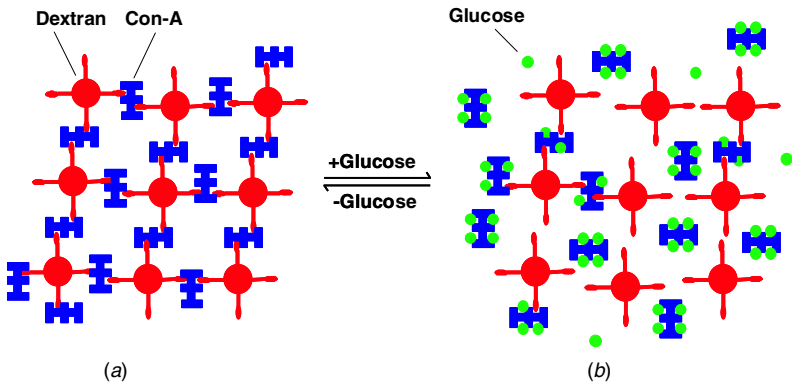

Figure 2. Schematic illustration of the affinity glucose sensing principle.

free glucose molecules enter the solution through the semi-permeable membrane from subcutaneous tissue, they will compete with the terminal glucose units of dextrans in binding to the Con A. The replacement of polymeric glucose on Con A by free glucose results in partial de-crosslinking of the dextran–Con A complex, consequently resulting in a decrease in the solution viscosity. This process is reversible, i.e., as the glucose concentration outside the membrane decreases, the glucose will unbind from Con A, causing the dextran crosslinking to recover and solution viscosity to increase. The competitive binding of free and polymeric glucose to Con A reaches an equilibrium when the glucose concentrations inside and outside the chamber are equalized. The solution viscosity under equilibrium conditions is thus a function of the glucose concentration in subcutaneous tissue. This function is independent of the extent to which the presence of the semi-permeable membrane hinders the diffusive transport of glucose. In particular, additional diffusion barrier layers on the membrane due to biofouling will not alter the functional relationship nor affect the accuracy of viscometric determination of glucose concentration.

The viscosity of the sensing solution is detected by vibration measurements. The device is placed in a magnetic field produced, for example, by a solenoid outside the skin. The magnetic field generates a torque in the permalloy film strips, which has the magnitude $T = VMH$. Here, V is the total permalloy volume, H is the magnetic field component perpendicular to the cantilever surface and M is the magnetization along the length of the permalloy strips. The torque is directed along the width of the cantilever, and causes cantilever bending. Thus, a time-dependent magnetic field generates a time-dependent torque, which in turn causes the cantilever to vibrate. The cantilever vibration is resisted by the elasticity of the cantilever, as well as the effects of vibration-induced flow of the solution. The flow effects on the vibration are manifested as apparent hydrodynamic inertia and damping [35], which directly depend on the solution viscosity. The measurement of the damped vibrations therefore allows determination of the sensing solution's viscosity.

3. Device model

Let the permalloy strips and the associated SU-8 reinforcement layer be collectively approximated as a rigid plate of mass

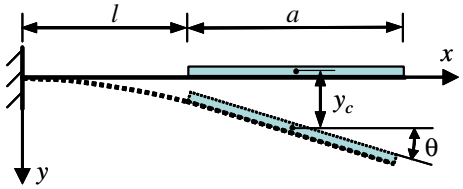

Figure 3. Geometry of the vibrating cantilever model.

m and length a, whose oscillation under the action of the magnetic torque involves translation y_c of the center of mass along the y-axis and rotation θ about the center of mass (figure 3). That is, the plate has two degrees of freedom, and it will be convenient to define a displacement vector, $q = [y_c, l\theta]^T$, where l is the cantilever length uncovered by the permalloy. The cantilever mass is negligible compared to m, and therefore can be represented as a massless elastic spring. From elastic beam theory, the spring force and torque are related to the plate displacement by $F_{el} = 12\left(y_c - \frac{1}{2}a\theta\right) - 6\theta$ and $T_{el} = -6\left(y_c - \frac{1}{2}a\theta\right) + 4\theta$, respectively, where $y_c - \frac{1}{2}a\theta$ is the deflection of the cantilever at its free end. The spring force vector, $R_{el} = [F_{el}, T_{el}/l]^T$, is hence given by $R_{el} = K_{beam}q$, where the cantilever stiffness matrix, K_{beam}, is given by

$$K_{beam} = k\begin{pmatrix} 12 & -6(1+a/l) \\ -6 & 4+3a/l \end{pmatrix}.$$

Here, $k = EI/l^3$, where E is Young's modulus and I is the cantilever's bending moment of inertia.

The force, F_f, and torque, T_f, exerted by the fluid flow on the plate must be determined by solving the associated fluid dynamics problem, which in general is difficult. However, these quantities are expected to be related to the plate's velocity and acceleration. In terms of a fluid force vector, $R_f = [F_f, T_f]^T$, we can write $R_f = M_f\ddot{q} + D_f\dot{q}$, where M_f is the added mass matrix and D_f is the fluid damping. While specific forms of these matrices for the cantilever immersed in a sensing solution are not yet available, reasonable approximations may be obtained for cantilever vibrations in air (section 6).

The oscillation of the plate is governed by the equations $m\ddot{y}_c = -F_{el} - F_f$ and $\frac{1}{12}ma^2\ddot{\theta} = -T_{el} + F_{el}\left(\frac{1}{2}a\right) - T_f - T_{mag}$. In the matrix form, they can be written as

$$(M + M_f)\ddot{q} + D_f\dot{q} + Kq = R_{mag} \qquad (1)$$

where the mass and stiffness matrices, along with the magnetic force vector, are given by

$$M = \begin{pmatrix} m & 0 \\ 0 & \frac{1}{12}m(a/l)^2 \end{pmatrix},$$
$$K = k\begin{pmatrix} 12 & -6(1+a/l) \\ -6(1+a/l) & 4+6(a/l)+3(a/l)^2 \end{pmatrix} \quad (2)$$
$$R_{\mathrm{mag}} = \begin{pmatrix} 0 \\ T_{\mathrm{mag}}/l \end{pmatrix}.$$

This 2-DOF problem can be analyzed with the method of modal analysis [36]. Consider the eigenvalue problem associated with the mass and stiffness matrices in equation (1). That is, we seek a scalar λ and a vector u such that the following equation holds:

$$[K - \lambda(M + M_{\mathrm{f}})]\,u = 0. \quad (3)$$

Two eigenvalues, λ_1 and λ_2, exist with associated eigenvectors u_1 and u_2, respectively. Assuming that the total mass and stiffness matrices are symmetric and positive definite, then $\lambda_1 > \lambda_2 > 0$ and u_1 and u_2 are real and orthogonal, i.e., ${u_1}^{\mathrm{T}} u_2 = 0$. Scale the eigenvectors such that they have unit magnitude: $|u_1| = |u_2| = 1$, and define a matrix by $U = [u_1\ u_2]$. It can be shown that this matrix has the following properties: $U^{\mathrm{T}}(M + M_{\mathrm{f}})U = \mathrm{diag}(m_1, m_2)$ and $U^{\mathrm{T}}KU = \mathrm{diag}(k_1, k_2)$, where $\mathrm{diag}(m_1, m_2)$ (or $\mathrm{diag}(k_1, k_2)$) is a 2×2 diagonal matrix with m_1 and m_2 (or k_1 and k_2) as the first and second diagonal elements (with m_1, m_2, k_1 and k_2 all positive). Thus, introducing a change of variables $q = Up$, equation (1) can be transformed to

$$\mathrm{diag}(m_1, m_2)\ddot{p} + U^{\mathrm{T}} D_{\mathrm{f}} U\dot{p} + \mathrm{diag}(k_1, k_2)p = U^{\mathrm{T}} R_{\mathrm{mag}}. \quad (4)$$

In general, the matrix $U^{\mathrm{T}} D_{\mathrm{f}} U$ is not diagonal. However, it may be approximated by a diagonal matrix $\mathrm{diag}(c_1, c_2)$, where c_1 and c_2 are positive real numbers. Then equation (4) represents two decoupled vibration modes:

$$m_i\ddot{p}_i + c_i\dot{p}_i + k_i p_i = u_i^{\mathrm{T}} R_{\mathrm{mag}} \quad (i = 1, 2). \quad (5)$$

It follows that m_i, c_i and k_i are the effective mass, and damping and spring coefficients of the ith vibration mode. In addition, $\omega_i = (k_i/m_i)^{1/2}$ is the ith fundamental frequency and u_i is the ith modal shape. Let the vibration modes be ordered such that $\omega_1 < \omega_2$. In the case where the first fundamental frequency is much lower than the second natural frequency, the vibration is dominated by the first mode. Thus, after $p_1(t)$ is found from equation (5) ($i = 1$), the displacement vector is approximately $q(t) = p_1(t)u_1$. The photodetector output is then given by $v_{\mathrm{out}}(t) = (r^{\mathrm{T}}u_1)p_1(t)$, where r is a constant vector determined by the optical lever setup and the positioning of the sensor.

According to this procedure, the cantilever vibration problem can be solved when the cantilever is subjected to either harmonic or transient excitation. For example, consider steady-state vibration under harmonic excitation $R_{\mathrm{mag}} = R_0 \mathrm{e}^{\mathrm{j}\omega t}$. The cantilever vibration is

$$p_1 = \frac{1}{\omega_1^2 - \omega^2 + 2\mathrm{j}\varsigma_1\omega_1\omega} m_1^{-1} u_1^T R_{\mathrm{mag}}, \quad (6)$$

where $\varsigma_1 = \frac{1}{2}c_1/\sqrt{m_1 k_1}$ is the damping ratio, which in general is a function of the excitation frequency ω due to the coupling of vibration with fluid flow. The system is said to be underdamped if $\varsigma_1 < 1/\sqrt{2}$, in which case resonance will occur, and overdamped if $\varsigma_1 > 1/\sqrt{2}$, in which case there is no resonance. This analysis will be applied below to interpret measured cantilever vibrations in air.

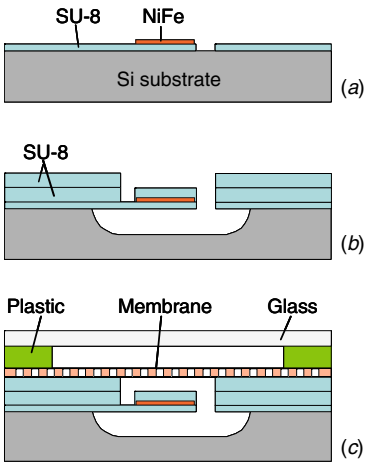

Figure 4. Device fabrication and assembly process.

4. Fabrication process

The device fabrication process (figure 4) started with deposition and patterning of a layer of SU-8 (7 μm) to form the cantilever (600 μm long and 500 μm wide). A permalloy film was sputter deposited and patterned to form eight strips each with dimensions $500 \times 50 \times 1$ μm^3 at the cantilever's free end (figure 4(*a*)). This was followed by the spin coating and patterning of two additional SU-8 layers (40 and 100 μm thick, respectively; figure 4(*b*)). These layers, along with the first SU-8 layer, formed the chamber's side walls (total height: 147 μm). In addition, a 500×500 μm^2 portion of the 40 μm thick layer directly covered the permalloy area to prevent curling of the cantilever due to stress mismatch between the permalloy and SU-8, as well as to isolate the permalloy from the sensing solution. Gas-phase XeF_2 etching was then used to release the cantilever by etching the silicon directly underneath it (figure 4(*b*)). The resulting chip was packaged to form a complete device assembly (figure 4(*c*)), with epoxy used as an adhesive in all bonding steps. Specifically, to form the inlet and outlet for the microchamber, two PEEK tubes (OD: 360 μm; ID: 150 μm) were each adhesive affixed horizontally in grooves that connected the microchamber and an edge of the substrate. (The grooves were formed within the SU-8 layers and the silicon substrate during microfabrication.) A semi-permeable membrane was bonded to form the top wall of the microchamber. The chamber, including the cavity XeF_2 etched into the silicon substrate, was estimated to be about $1 \times 1 \times 0.4$ mm^3 (0.4 μL) in volume. Finally, a test flow cell about 20 μL in volume was formed on top of the membrane by bonding a plastic spacer disk and a glass cover slip. The inlet and outlet for the test cell were provided via adhesive-affixed PEEK or rubber tubes. Images of a fabricated device before and after packaging are shown in figure 5.

In general, the semi-permeable membrane must meet several requirements. The membrane's pore diameter must be sufficiently large to allow the passage of glucose molecules, and also small enough to prevent the passage of the active components (i.e., Con A and dextran) in the sensing solution. Moreover, the membrane should have a relatively small thickness and large porosity, so that the diffusive glucose flux is sufficiently large at physiologically relevant concentration

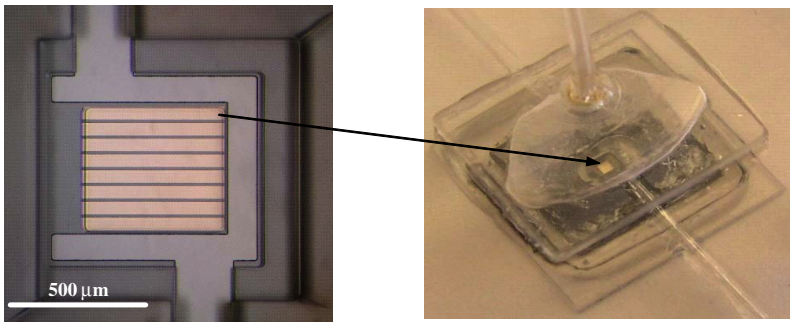

(*a*) (*b*)

Figure 5. Image of a device (*a*) before cantilever released by XeF_2 etching and (*b*) after packaging and filling of the sensing solution.

differences at the two sides of the membrane. This is necessary for the glucose concentration to equilibrate within an adequately small time period, which essentially determines the device's response time. Our prototype devices used three different membranes, two of which were regenerated cellulose acetate (CA) membranes (Pierce Biotechnology) each 12 μm in thickness, with 10 and 3.5 kD molecular weight cutoffs (MWCO), respectively. The third membrane was a polycarbonate track etched (PCTE) membrane with 10 nm pore diameter and 10 μm thickness (Sterlitech Corporation). In principle, glucose (molecular weight: 180 Da and hydrodynamic diameter: 1.5 nm) would be able to freely permeate through the membranes, which should prevent the permeation of Con A (molecular weight: 103 kD and size: approximately $6 \times 7 \times 7$ nm^3) and dextran (molecular weight: 500 kD and hydrodynamic diameter: 30 nm).

5. Experimental method and setup

Chemicals and reagents used in the experiments include glycerol (Sigma–Aldrich), Con A (Sigma–Aldrich), dextran (Dextran-500, Fisher Scientific) and glucose (Alpha-d-(+)-Glucose, Acros). Phosphate buffer saline solution (PBS), pH 7.0, was made of potassium phosphate (20 mM, or mmol L^{-1}), NaCl (150 mM) and NaN_3 (0.05%). Dextran solution was prepared by dissolving dextran (1.0 g) in PBS to 5.0 mL volume. Likewise, Con A (200.0 mg) was dissolved in PBS to 5 mL, followed by the addition of $MnCl_2{\cdot}4H_2O$ (4.0 mg) and $CaCl_2$ (2.0 mg) to increase the solution's complexibility. The sensing solution was then prepared by mixing dextran (50.0 mg mL^{-1}) and Con A (10.0 mg mL^{-1}) solutions.

Glucose stock solution (1.0 M) was prepared by dissolving glucose (1.8 g) in PBS to 10.0 mL. A series of glucose solutions (3.0, 6.0, 12.0, 18.0 and 25.0 mM) were prepared by dilution of the stock solution with PBS. To prepare sensing solutions premixed with glucose (hereafter referred to as 'premixed samples'), solutions of dextran (50.0 mg mL^{-1}), Con A (10.0 mg mL^{-1}) and glucose (at one of the concentrations above) were mixed together.

Measurements of sensing solution viscosity at varying glucose concentrations were performed with capillary viscometers (Cannon Instrument Company, models 9722-H50 and 9722-H62), which were equipped with a water bath with temperature maintained at 37 °C. All experiments with MEMS prototype devices were also conducted at 37 °C with temperature control provided by a thermoelectric heater. This was necessary as viscosity of fluids is temperature dependent. In experiments using glycerol solutions, glycerol diluted to desired concentrations (10% and 20%) were prepared and used to fill the microchamber and test cell using syringe pumps connected to the appropriate inlet tubes. Experiments using glucose solutions were performed according to two methods. First, both the microchamber and test cell were filled with premixed samples of the same glucose concentration, and then cantilever vibration measurements were performed. In these experiments, hereafter called 'pre-equilibrated' measurements, the glucose concentration in the chamber did not vary with time and was determined from that of premixed samples. In the second type of experiments, the samples in the chamber and test cell had different glucose concentrations; because the volume of the test cell was 50 times that of the chamber, it was reasonable to assume that the glucose concentration in the chamber would eventually equal that in the test cell, which did not vary with time. These experiments, referred to as 'permeation measurements', simulate the operation of an implantable glucose sensor involving diffusive transport of glucose between two sides of the semi-permeable membrane.

The cantilever vibration was driven by a home-made solenoid (400 turns of a 250 μm diameter copper wire on a plastic core), which, under a driving voltage of 5 V_{rms}, produced a magnetic field strength of about 950 A m^{-1} perpendicular to the cantilever surface. A permanent magnetic bar with a field strength of 200 kA m^{-1} was placed parallel to the cantilever surface to allow saturated magnetization of the permalloy strips.

To measure cantilever vibrations, an optical lever system was used (figure 6). A laser beam from a laser diode (Coherent, Inc., model P/N 31-0235) was directed onto the permalloy surface on the cantilever. The reflected light was detected by a photodetector equipped with an amplifier (On-Trak Photonics, Inc., model PSM2-4 and model OT-301). The cantilever deflection changed the path of the reflected light. The resulting changes in the reflected light spot position on the photodetector surface caused changes in the photodetector output, which was detected by a lock-in amplifier (for measuring harmonic vibrations) or an oscilloscope connected to a PC (transient vibrations). Thus, in all experimental results below, the cantilever deflection will be presented in terms of the output voltage from the lock-in amplifier or oscilloscope.

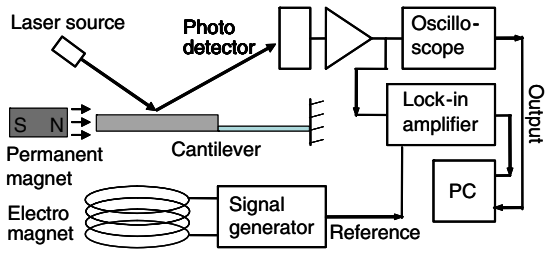

Figure 6. Experimental setup for characterization of the MEMS glucose sensor. The cantilever vibration is measured with an optical lever system.

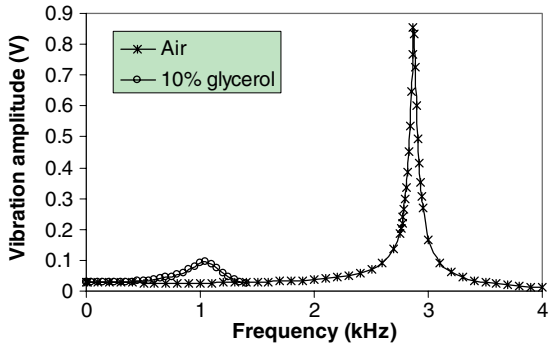

Figure 7. Amplitude of cantilever vibration (in terms of the lock-in amplifier output) in air under a harmonically varying magnetic field.

6. Results and discussion

This section presents the experimental results from the fabricated devices. We first investigate the dynamic characteristics of the cantilever by examining its vibration in air, and then discuss the choice of semi-permeable membrane, which critically influences the device's time response. Cantilever vibration measurements involving glucose permeating through the semi-permeable membrane at varying concentrations are finally presented. We have tested a total of twelve devices, all of which showed results that were qualitatively similar. Therefore, results from three devices, which had the same nominal dimensions as given in section 4 except different semi-permeable membrane choices, are presented below.

6.1. Cantilever vibration characteristics

To characterize the properties of the cantilever, we measured the cantilever vibration in air when a sinusoidally varying voltage (amplitude: 0.5 V) was applied to the solenoid. The measured vibration amplitude as a function of excitation frequency showed pronounced resonance (figure 7). The slight decrease of amplitude to values below static deflection (corresponding to frequency equal to zero) at frequencies up to 1.5 kHz may be attributed to the moderate decrease of the magnetic field magnitude with increasing frequency due to self-induction effects of the solenoid coil. The Q factor for the resonance peak was determined to be about 57, which is sufficiently large to justify the approximation that the resonance frequency (2.87 kHz) equals the basic natural frequency of the cantilever system.

To obtain a theoretical understanding, we apply equation (1) to this case of cantilever vibration. Using dimensions given in section 4 and typical material properties of SU-8 (Young's modulus: 4 GPa and density: 1200 kg m^{-3}) and permalloy (density: 8740 kg m^{-3}), we obtain $m = 16.8\ \mu g$ and $k = 62.2$ N m^{-1}. Because the density of air (1.16 kg m^{-3}) is about 1000 times smaller than that of SU-8, the added mass due to air flow can be neglected. The natural frequencies of the cantilever system can be determined by considering its free vibration without inclusion of damping: $M\ddot{q} + Kq = 0$, where the mass (in μg) and stiffness (in N m^{-1}) matrices are, respectively, evaluated according to equation (2) to be

$$M = \begin{pmatrix} 16.8 & 0 \\ 0 & 35.0 \end{pmatrix}, \qquad K = \begin{pmatrix} 746.5 & -2239 \\ -2239 & 6780 \end{pmatrix}.$$

The eigenvalues as defined in equation (3) can be found to be $\lambda_1 = 3.321 \times 10^8$ and $\lambda_2 = 2.378 \times 10^{11}$ rad^2 s^{-2}, which can be used to compute the cantilever's natural frequencies: $f_1 = \frac{1}{2\pi}\lambda_1^{1/2} = 2.90$ kHz and $f_2 = \frac{1}{2\pi}\lambda_2^{1/2} = 77.6$ kHz. The calculated basic natural frequency of 2.90 kHz agrees well with the measured resonance frequency of 2.84 kHz. In addition, as f_2 is an order of magnitude larger than f_1, the first vibration mode dominates.

6.2. Effects of the semi-permeable membrane choice on device time response

As mentioned in section 4, semi-permeable membranes of three different specifications were used to construct prototype devices. We evaluated how the different permeability of these membranes impacts the device time response by testing the devices with glycerol solutions. The use of glycerol solutions, which are Newtonian fluids, also served to corroborate the sensor's capability to detect viscosity changes via vibration damping measurements. Under harmonic magnetic excitations, the frequency dependence of cantilever vibration in relatively low-concentration glycerol solutions (10% and 20%, respectively, with viscosities 1.3 and 1.6 cP at room temperature) was observed to exhibit resonance behavior similar to that observed in air (figure 7), although with a much more broadened resonance peak due to significant hydrodynamic damping. The resonance frequency (around 1.05 kHz) was much lower than that in air, as the solution, with a comparable density to SU-8, contributed a significant added mass to the vibration (equation (1)).

When using different glycerol concentrations in the microchamber (20%) and test cell (10%), the process of glucose concentration equalization on the two sides of the semi-permeable membrane could be observed to determine the device's time response. This was conveniently accomplished by monitoring the time-dependent phase shift of the cantilever vibration relative to a harmonic magnetic excitation, as is shown in figure 8 (frequency: 1.45 kHz). It can be seen that the measurement data for all three semi-permeable membrane choices can be well represented by a first-order system, with time constants of 4.27 (CA membrane with 10 kD MWCO), 15.6 (CA membrane with 3.5 kD MWCO) and 42.65 (PCTE membrane with 10 nm pores) min, respectively. It follows that the CA membrane with 10 kD MWCO offered the fastest time response that lies within a practically relevant range for continuous glucose monitoring.

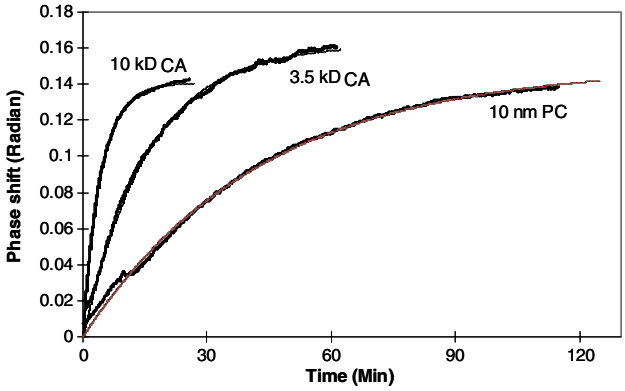

Figure 8. Time-dependence of the phase shift of cantilever vibration under a harmonic magnetic excitation (thick lines: measurement; thin lines: fitting), with different semi-permeable membrane choices. The microchamber was initially filled with a 20% glycerol solution and the test cell with a 10% glycerol solution.

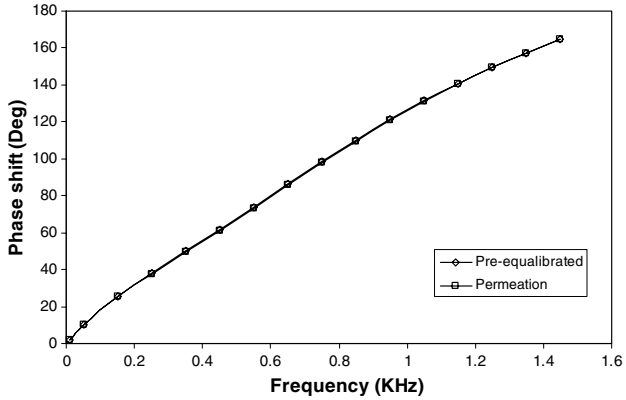

Figure 10. Comparison of measurement results from pre-equilibrated and permeation experiments leading to a final glucose concentration of 6 mM in the microchamber. The cantilever vibration was excited by a harmonically time-varying magnetic field.

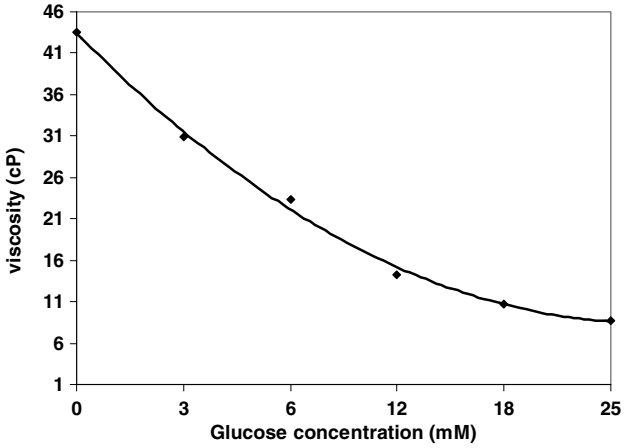

Figure 9. Viscosity of sensing solutions mixed with glucose at physiologically relevant concentrations.

6.3. Glucose measurements

We first measured the viscosity of sensing solutions mixed with glucose at varying concentrations using capillary viscometers at 37 °C (figure 9). It shows that glucose indeed induced significant changes in the viscosity of the sensing solution. As the glucose concentration varied from 0 to 25 mM, the viscosity changed from 43.4 to 8.72 cP. This glucose concentration range is physiologically relevant, and consistent with concentration ranges of commercially available CGM devices (e.g., 2.2–22.2 mM [6, 8]).

Glucose measurements were then carried out. Presented below are the results obtained using a prototype MEMS viscometric sensor equipped with a CA membrane with 10 kD MWCO. Permeation measurements were first compared with pre-equilibrated measurements (section 5) to verify the achievement of concentration equalization and equilibrium binding of glucose to Con A. Typical results are shown in figure 10 in terms of the frequency-dependent vibration phase shift. The pre-equilibrated measurements involved placing premixed samples of the same glucose concentration (6 mM) in the microchamber and the test cell. In the permeation measurements, the glucose concentration was initially zero in the chamber and 6 mM in the test cell. It can be observed from figure 10 that agreement between the two types of measurements is satisfactory. As the frequency is varied from 0 to 1.45 kHz, the pre-equilibrated and permeation experimental results differ by less than 3% over the entire frequency range. In addition, while the data is not shown, there is a similar agreement between the two types of measurements for the cantilever's amplitude frequency response to harmonic excitations, as well as transient response to step excitations. This verifies that equilibrium was achieved in the permeation experiments.

Permeation measurements at varying glucose concentrations were then conducted with harmonic cantilever vibrations. In the experiments, the sensing solution initially did not contain glucose. Glucose solutions of increasing concentrations were consecutively passed through the test cell. At each glucose concentration, when glucose permeation through the membrane had achieved equilibrium, three frequency sweeps were performed for the voltage applied on the solenoid, and the amplitude and phase were measured. The three sets of data were then averaged and presented in figures 10 and 11. The vibration amplitude can be observed to increase with glucose concentration at any given frequency. This agrees with the decreased viscosity and damping at higher glucose concentrations due to de-crosslinking of dextran. There exists a range of frequencies, approximately from 350 to 650 Hz, over which the vibration amplitude changed most significantly with glucose concentration. For example, at 550 Hz, the sensitivity of the photodetector output with respect to the glucose concentration change increased from 2.3 mV mM^{-1} at 25 mM to 5.6 mV mM^{-1} at 3 mM.

The shape of the amplitude frequency response curves in figure 11 differs significantly from the case of cantilever vibration in air (figure 7). This is primarily because of the highly viscous nature of the sensing fluid, which led to large damping on the cantilever vibrations. It should be noted, however, that at high glucose concentrations, the vibration is still weakly resonant, at a frequency much lower than the basic natural frequency of 2.84 kHz. The smaller resonance

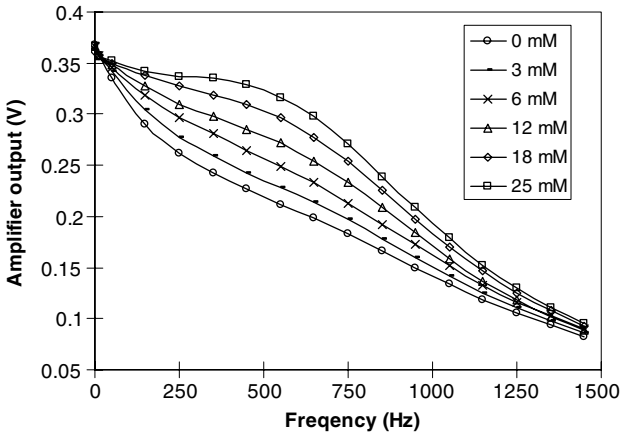

Figure 11. Frequency dependence of the cantilever vibration amplitude due to a harmonically time-varying magnetic field.

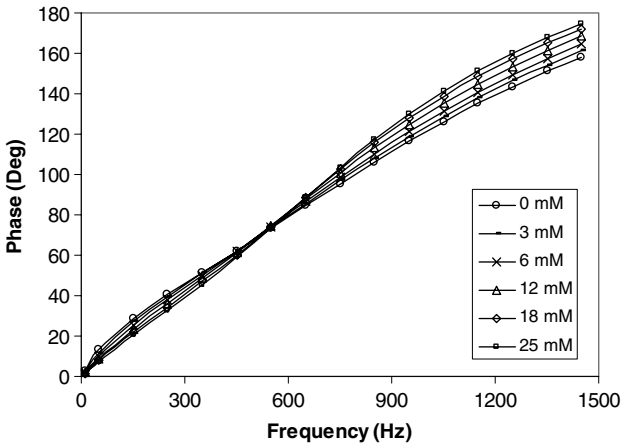

Figure 12. Frequency dependence of the cantilever vibration phase shift due to a harmonically time-varying magnetic field.

frequency can be explained by the large added mass (equation (1)) due to the flow of the sensing fluid.

From the phase response curves (figure 12), the phase of vibration was nearly 0° at the lower frequencies, which is consistent with the quasistatic nature of vibration. As the frequency increased, the phase shift consistently increased, approaching 180° at the upper end of the spectrum. As the glucose concentration increased, the viscosity and damping decreased. At a fixed frequency below 550 Hz, at which the phase curves crossed over, the phase shift increased with decreasing glucose concentration or increasing damping. The cross-over occurs at the effective basic natural frequency, indicating that the added mass lowered the basic frequency from 2.84 kHz to 550 Hz. The phase shift at the crossover was about 74°, which differs from the value (90°) predicted by the linear oscillator theory. This most likely could be attributed to extraneous phase shifts in the electronics of the measurement instruments. At a fixed frequency above 550 Hz, the phase shift decreased with decreasing glucose concentration or increasing damping. For example, at 1.45 kHz, the sensitivity of phase shift with respect to glucose concentration changes ranged from 1.1° mM^{-1} (at 0 mM) to 0.4° mM^{-1} (at 18 mM). With the lock-in amplifier's capability to resolve phase changes down

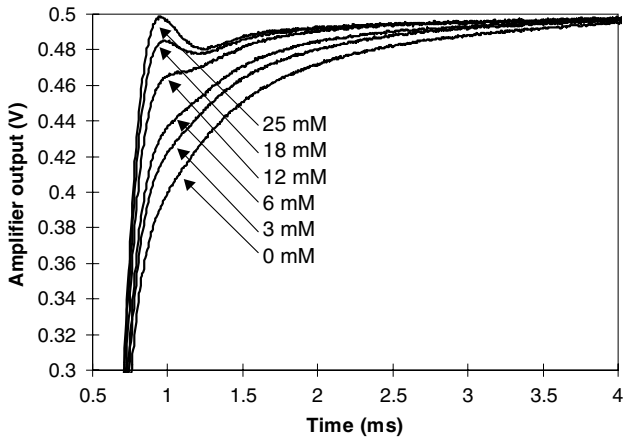

Figure 13. Cantilever deflection under a suddenly applied constant magnetic field.

to 0.01°, the phase measurements would allow a measurement resolution of 0.025 mM in glucose concentration.

We have also measured transient cantilever vibrations. The cantilever vibration in response to a step voltage (10 V) applied to the solenoid is shown in figure 13. This transient response varied also significantly with the glucose concentration. At any time, the cantilever deflection increased with glucose concentration as a result of decreases in damping, which were caused by reduced viscosity. For the same reason, the vibration was overdamped at the lower glucose concentrations. At higher glucose concentrations, the system became underdamped and the vibration slightly exhibited second-order, oscillatory behavior.

Finally, we investigated the reversibility of glucose sensing by the prototype device. Under either a harmonic or step magnetic excitation, the device was tested with the glucose concentration in the test cell cycling between two values, e.g., 3 and 12 mM. It was observed that changes of cantilever vibration characteristics were generally reversible. For example, when the glucose concentration varied from 3 to 12 mM, the phase shift decreased by approximately the same amount (6.732°) as the phase shift increased (6.729°) due to a glucose concentration variation from 12 to 3 mM. Thus, the MEMS viscometric sensor is relevant to practical applications, where both increasing and decreasing glucose concentrations must be detected.

In these experiments, drift (on the order of up to 15% per hour) was observed in the final values of the phase shift for each cycle of glucose concentration variation. Drift was also present when the sensor response was monitored for an extended period of time at a fixed glucose concentration in the test cell. Preliminary UV absorption measurements in our ongoing work have suggested that there was no significant leakage of Con A through the CA membrane. Therefore, Con A leakage likely was not the main cause for the drift. On the other hand, osmosis effects might be a more likely cause. The volume fraction of water in the test cell, with the absence of Con A and dextran molecules, was much higher than that in the microchamber. Thus, water might have diffused into the microchamber via osmosis [37], causing the dilution of the sensing solution and decrease of viscosity and vibration damping. This could be addressed by improved preparation

of the sensing and testing solutions so that they are isotonic, or have the same water volume fractions. Furthermore, it is worth noting that in clinical applications, osmosis effects would reach equilibrium so that drifts would exist only in a limited time period following sensor implantation.

7. Conclusions

A MEMS viscometric glucose sensor has been developed. The device consists of an SU-8 microcantilever coated with a permalloy thin film, which is located in a microfluidic chamber (also fabricated from SU-8) and vibrates in a remotely applied magnetic field. The sensing fluid, consisting of the polymer dextran and the protein Con A, exchanges glucose with the fluid outside the device through a cellulose acetate semi-permeable membrane. The damping on the cantilever vibration depends on the viscosity of the sensing fluid, which in turn is determined by the interaction of glucose with Con A. Thus, the cantilever vibration can be measured to obtain the glucose concentration. The dynamic characteristics of the device have been characterized with the cantilever vibrating in air and glycerol solutions. A model has been developed to show that the vibrating cantilever can be represented as a two-degree-of-freedom system. The device time response has also been found to be practically relevant (down to 4.27 min), and can be further improved with optimized designs. Glucose measurements have been successfully performed with the device at physiologically relevant concentrations (0 to 25 mM), with the glucose-induced viscosity change detected either by steady-state or transient cantilever vibrations. These measurements have shown that the cantilever vibration is quite sensitive to glucose concentrations. For example, the sensitivity of the phase of steady-state response was greater than 0.4° mM^{-1}, suggesting a measurement resolution of 0.025 mM in glucose concentration. The device represents a first step toward an implantable MEMS sensor that is miniaturized and affords the excellent stability offered by non-consumptive equilibrium binding principles.

A number of issues can be considered in future work. First, simulations of the cantilever vibration in the sensing solution would yield valuable insights into the viscometric affinity sensing approach as well as device design guidelines. The main challenge to be addressed will be the tight coupling between the cantilever vibration and fluid flow. Harmonic vibrations will likely be more tractable than transient vibrations, as the vibration and flow equations could be formulated in the frequency domain and solved using a numerical partial differential equation solver without computationally expensive time integration. Second, improved device designs can be generated, for example, to include electronic sensing and more rapid time response. For sensors with configurations shown in figure 1, thin-film piezoresistive strain gauges would be a natural choice for electronic sensing. The device time response can be improved by reducing the microchamber height to reduce glucose diffusion distances, and by the combined use of more porous semi-permeable membranes and suitable sensing solutions. Finally, drifts in sensor responses should be addressed. This may include thorough Con A diffusion studies to rule out the leakage of Con A through the regenerated cellulose acetate membrane. Then, isotonic sensing and testing solutions can be prepared and used in device testing, to verify that the drifts observed in this work were indeed caused by osmosis effects and can thus be effectively eliminated by suppression of osmosis.

Acknowledgments

We wish to thank Drs R Ballerstadt and J S Schultz for discussions on the Con A/dextran system, as well as Dr J A Bain for discussions on magnetic thin films. The work has been supported by NASA (contract #NAG8-1799), NSF (grant #ECCS-0702101), and the Columbia Diabetes and Endocrinology Research Center (NIH grant #DK63068-05).

References

[1] Klonoff D C 2007 Subcutaneous continuous glucose monitoring in severe burn patients *Crit. Care Med.* **35** 1445
[2] Koschinsky T and Heinemann L 2001 Sensors for glucose monitoring: technical and clinical aspects *Diabetes-Metab Res. Rev.* **17** 113–23
[3] Pickup J C, Hussain F, Evans N D, Rolinski O J and Birch D J S 2005 Fluorescence-based glucose sensors *Biosensors Bioelectron.* **20** 2555–65
[4] Heller A 1999 Implanted electrochemical glucose sensors for the management of diabetes *Annu. Rev. Biomed. Eng.* **1** 153–75
[5] Abbott Diabetes Care *Freestyle Navigator® Continuous Glucose Monitoring System* http://www.abbottdiabetescare.com
[6] Medtronic MiniMed *Guardian® Real-Time Continuous Glucose Monitoring System* http://www.minimed.com/products/guardian/index.html
[7] Medtronic MiniMed *Minimed Paradigm® Real-Time Insulin Pump and Continuous Glucose Monitoring System* http://www.minimed.com/products/insulinpumps/index.html
[8] DexCom, Inc. *Dexcom(tm) STS® System* http://www.dexcom.com/
[9] Menarini A Diagnostics *Glucoday® S* http://www.menarini.com/english/diagnostica/glucoday_00a.htm
[10] Ballerstadt R and Ehwald R 1994 Suitability of aqueous dispersions of dextran and concanavalin A for glucose sensing in different variants of the affinity sensor *Biosensors Bioelectron.* **9** 557–67
[11] Ballerstadt R, Gowda A and McNichols R 2004 Fluorescence resonance energy transfer-based near-infrared fluorescence sensor for glucose monitoring *Diabetes Technol. Ther.* **6** 191–200
[12] Beyer U, Schafer D, Thomas A, Aulich H, Haueter U, Reihl B and Ehwald R 2001 Recording of subcutaneous glucose dynamics by a viscometric affinity sensor *Diabetologia* **44** 416–23
[13] Ehwald R, Ballerstadt R and Dautzenberg H 1996 Viscosimetric affinity assay *Anal. Biochem.* **234** 1–8
[14] Mansouri S and Schultz J S 1984 A miniature glucose sensor based on affinity binding *Biotechnol.* **2** 885–90
[15] Meadows D L and Schultz J S 1993 Design, manufacture and characterization of an optical fiber glucose affinity sensor based on a homogeneous fluorescence energy transfer assay system *Anal. Chim. Acta* **280** 21–30
[16] Schultz J S and Sims G 1979 Affinity sensors for individual metabolites *Biotechnol. Bioeng. Symp.* **9** 65–71
[17] Schultz J S, Mansouri S and Goldstein I J 1982 Affinity sensor—a new technique for developing implantable

sensors for glucose and other metabolites *Diabetes Care* **5** 245–53
[18] Beyer U, Ehwald R and Fleischer L-G 1997 Post-stress thickening of dextran/concanavalin A solutions used as sensitive fluids in a viscosimetric affinity assay for glucose *Biotechnol. Prog.* **13** 722–6
[19] Beyer U and Ehwald R 2000 Compensation of temperature and concanavalin A concentration effects for glucose determination by the viscometric affinity assay *Biotechnol. Prog.* **16** 1119–23
[20] Jeckelmann J and Seibold A 2002 Gluconline *Diabetes Profile*
[21] Diem P, Kalt L, Haueter U, Krinelke L, Fajfr R, Reihl B and Beyer U 2004 Clinical performance of a continuous viscometric affinity sensor for glucose *Diabetes Technol. Ther.* **6** 790–9
[22] Cai X X, Glidle A and Cooper J M 2000 Miniaturized electroanalytical sensor systems in micromachined structures *Electroanalysis* **12** 631–9
[23] Kurita R, Hayashi K, Fan X, Yamamoto K, Kato T and Niwa O 2002 Microfluidic device integrated with pre-reactor and dual enzyme-modified microelectrodes for monitoring *in vivo* glucose and lactate *Sensors Actuators* **87** 296–303
[24] Park S I, Jun S B, Park S, Kim H C and Kim S J 2003 Application of a new Cl-plasma-treated Ag/AgCl reference electrode to micromachined glucose sensor *IEEE Sensors J.* **3** 267–73
[25] Wu J, Suls J and Sansen W 2001 The glucose sensor integratable in the microchannel *Sensors Actuators* B **78** 221–7
[26] Wang J, Chatrathi M P, Tian B M and Polsky R 2000 Microfabricated electrophoresis chips for simultaneous bioassays of glucose, uric acid, ascorbic acid and acetaminophen *Anal. Chem.* **72** 2514–8
[27] Xie B, Ramanathan K and Danielsson B 2000 Mini/micro thermal biosensors and other related devices for biochemical/clinical analysis and monitoring *Trends Anal. Chem.* **19** 340–9
[28] Bataillard P 1993 Calorimetric sensing in bioanalytical chemistry: principles, applications and trends *Trends Anal. Chem.* **12** 387–94
[29] Zhang Y Y and Tadigadapa S 2004 Calorimetric biosensors with integrated microfluidic channels *Biosensors Bioelectron.* **19** 1733–43
[30] Pu C, Zhu Z H and Lo Y H 2000 A surface-micromachined optical self-homodyne polarimetric sensor for noninvasive glucose monitoring *IEEE Photonics Technol. Lett.* **12** 190–2
[31] Paranjape M, Garra J, Brida S, Schneider T, White R and Currie J 2003 A PDMS dermal patch for non-intrusive transdermal glucose sensing *Sensors Actuators* A **104** 195–204
[32] Zahn J D, Trebotich D and Liepmann D 2000 Microfabricated microdialysis microneedles for continuous medical monitoring *Proc. 1st IEEE EMBS Joint Conf. Microtechnol. Biol. Med.* pp 375–80
[33] Lin Y, Matson D W, Kurath D E, Wen J, Xiang F, Bennett W D, Martin P M and Smith R D 2000 Microfluidic devices on polymer substrates for bioanalytical applications *Microreaction Technology: Industrial Prospects* ed W Ehrfeld (Berlin: Springer-Verlag) pp 451–60
[34] Lei M, Baldi A, Nuxoll E, Siegel R A and Ziaie B 2006 A hydrogel-based implantable micromachined transponder for wireless glucose measurement *Diabetes Technol. Ther.* **8** 112–22
[35] Landau L D and Lifshitz E M 1987 *Fluid Mechanics* 2nd edn (Oxford: Pergamon Press)
[36] Weaver W, Timoshenko S P and Young D H 1990 *Vibration Problems in Engineering* 5th edn (New York: Wiley)
[37] Katchalsky A and Curran P F 1965 *Nonequilibrium Thermodynamics in Biophysics* (Cambridge, MA: Harvard University Press)